Available online at www.sciencedirect.com
ScienceDirect
Optics Communications 277 (2007) 14–18
OPTICS COMMUNICATIONS
www.elsevier.com/locate/optcom

Measurement of the thermal expansion coefficients of ferroelectric crystals by a moiré interferometer

F. Pignatiello [a,b], M. De Rosa [a,b,*], P. Ferraro [a,b], S. Grilli [a,b], P. De Natale [a,b], A. Arie [c], S. De Nicola [d]

[a] CNR, Istituto Nazionale di Ottica Applicata, Sezione di Napoli, Via Campi Flegrei 34, 80078 Pozzuoli (NA), Italy
[b] LENS, European Laboratory for Non-linear Spectroscopy, Via Campi Flegrei 34, 80078 Pozzuoli (NA), Italy
[c] Department of Physical Electronics, School of Electrical Engineering, Faculty of Engineering, Tel-Aviv University, Tel-Aviv 69978, Israel
[d] CNR, Istituto di Cibernetica "E.Caianiello", Via Campi Flegrei 34, 80078 Pozzuoli (NA), Italy

Received 29 December 2006; received in revised form 20 April 2007; accepted 27 April 2007

Abstract

A moiré interferometer is used to measure the thermal expansion of two ferroelectric crystals, $LiNbO_3$ and $KTiOPO_4$. The crystal samples are patterned with a chromium reflective grating and used as a diffractive component in a reflective grating interferometer. The thermal expansion of all the three axes of congruent $LiNbO_3$ and of x and y axes of the flux-grown $KTiOPO_4$ were measured from room temperature to 200 °C. For this temperature range the thermal expansion coefficient has been modeled by a second-order polynomial and its coefficients have been estimated by accurate analysis of the resulting moiré fringe pattern.

Keywords: Moiré interferometry; Ferroelectric; Thermal expansion

1. Introduction

Lithium niobate ($LiNbO_3$) and potassium titanyl phosphate ($KTiOPO_4$ or shortly KTP) are two ferroelectric crystals of great interest for optoelectronic applications such as electro-optic and acousto-optic modulation or for nonlinear optics applications, such as second harmonic generation, difference frequency generation, optical parametric oscillators, etc. [1–3]. New devices are based on crystals with periodic modulation of the nonlinear coefficient, thus increasing the efficiency of nonlinear processes by quasi-phase-matched interactions [4–6]. Design of such devices requires accurate knowledge of the relevant physical parameters as a function of wavelength and temperature. As far as thermal expansion is concerned, it affects the optical path of the light passing through the devices, and its knowledge can be needed for determining other properties, as the thermo-optic coefficients [7]. Furthermore, in quasi-phase-match nonlinear processes thermal expansion changes the effective period of the nonlinear coefficient, and thus changes the phase matching condition. Moreover, density variations caused by thermal expansion contribute to thermally induced variation of acoustic waves velocity, crucial for frequency and signal control applications. Various experimental data were reported in literature for both crystals, based on different methods – namely, X-ray diffraction, interferometry, and capacitance dilatometer. However, for most of the values reported for $LiNbO_3$ the composition of the crystal was not reported [8,9], while for the KTP there is still a lack of accurate measurements and the values commonly reported are rather conflicting. The values reported in literature for KTP are limited to only the first-order coefficient, measured by different methods and for different temperature ranges [10,11]. A more recent work reports also the second-order coefficient, even though only for the x-axis [12].

* Corresponding author. Address: CNR, Istituto Nazionale di Ottica Applicata, Sezione di Napoli, Italy.
E-mail address: maurizio.derosa@inoa.it (M. De Rosa).

0030-4018/$ - see front matter © 2007 Elsevier B.V. All rights reserved.
doi:10.1016/j.optcom.2007.04.045

In this paper we present an interferometric measurement of the thermal expansion coefficients for several samples of $LiNbO_3$ and KTP crystals, from room temperature up to 200 °C. The measurement is based on moiré interferometry [13] and adopts a reflective grating optical configuration (reflective grating interferometer, RGI) [14,15]. A grating is fabricated onto the crystal sample and used as a diffractive component of the RGI. The interferometer gives rise to a fringe pattern whose spacing depends on the period of the grating lines which in turn depends on the expansion of the substrate. We performed measurements for a z-cut sample of KTP thus measuring the thermal expansion for x- and y-axis, and on both x- and z-cut samples of congruent $LiNbO_3$, being able to estimate the thermal coefficient along all the principle crystal axes. This method has been shown to be reliable for determination of thermo-mechanical strain and has been previously applied to the measurement of thermal expansion of electronic components [16,17]. It is suitable for small sample and as for other optical methods, mechanical interaction with the sample is strongly reduced, with no need of reference materials or mechanical parts which transduce the dilatation as for many mechanical or capacitive dilatometer. However the sample requires a grating to be written on it, which must follow the substrate expansion.

2. Experimental setup

The samples of $LiNbO_3$ are 0.5-mm-thick, x- and z-cut, congruent crystal, while for KTP we used a 0.5-mm-thick z-cut, flux-grown crystal. The main dimensions of the sample are around 10 mm × 10 mm. For each sample we wrote two reflective diffraction gratings ($\sim 7 \times 1$ mm^2) on the large face (i.e., x and z side for x- and z-cut sample respectively), with lines perpendicular to the remaining crystal axes directions respectively (inset a of Fig. 1). The gratings were written by electron-beam lithography as follows. The sample was coated with a 100-nm-thick layer of chromium and successively coated with a electron resist layer. The grating pattern was written with a Raith 150 electron-beam lithography system. The electron resist is developed and the chrome layer is etched through the developed resist. After removing the residual resist, a chromium grating is left. As checked by using an atomic force microscope, Fig. 2, the grating is made of chromium lines alternating to chromium-free crystal region, and the chromium lines are not connected each other, except at the boundary of the grating. So, we can reasonably assume that the grating follows faithfully the substrate expansion, independently of its orientation with respect to the crystal axes. The grating periods were checked both by microscope inspection and determined by measuring the diffraction angle by shining He–Ne laser radiation, thus getting 790 ± 1 nm for the x oriented grating of the KTP sample, and 800 ± 1 nm for all the remaining gratings. The choice of the grating period was merely dictated by the geometry of the setup, which requires incidence angles on mirror and grating of ~45°.

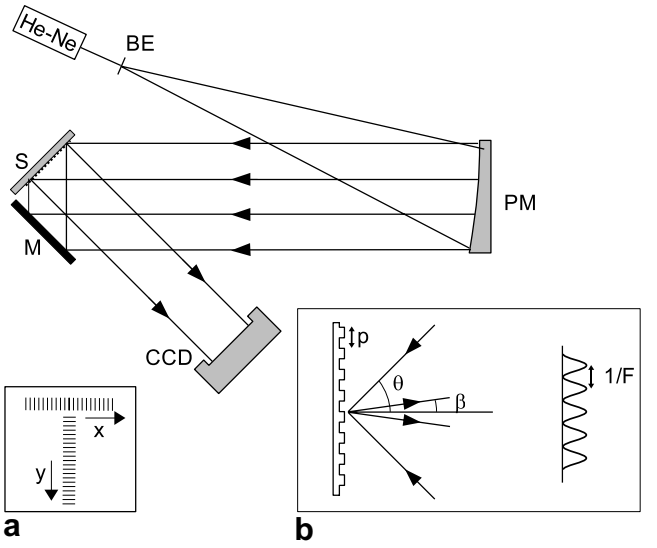

Fig. 1. Experimental setup. S: crystal sample; BE: beam expander; CCD: camera; M: mirror; PM: off-axis parabolic mirror. Inset (a) shows the sample with the two orthogonal gratings, while inset (b) shows a scheme of the moiré fringe pattern formation (see the text).

The crystal sample is placed on a temperature-controlled heater which can be heated up to 200 °C by means of four resistive heaters (dissipating 15 W at 12 V) buried inside an aluminum base. A copper holder is used for fixing the crystal sample and making a uniform thermal contact. The holder is actively stabilized within 0.1 °C by means of a home-made servo electronics. The heater is enclosed into an temperature insulating box in order to reduce air thermal dispersion and environmental perturbations. The light access onto the crystal sample is insured by appropriate openings of the box. A negative-temperature-coefficient (NTC) probe is embedded in the sample holder and is used for getting the error signal of the servo electronics. The crystal temperature is independently probed by a Pt100 sensor placed directly on the patterned side of the crystal, which is exposed to air. The difference between the temperature of the NTC, i.e., the back face of the crystal, and the temperature measured by the Pt100 on the front face of the crystal is within the uncertainty of the two sensors when the temperature is stabilized, so we assume that no remarkable temperature gradient occurs through the thickness of the sample.

The optical setup is sketched in Fig. 1. A collimated and linearly-polarized He–Ne laser, emitting 15 mW at $\lambda = 632.8$ nm, is expanded by the beam expander BE and collimated by a 10-cm-diameter off-axis parabolic mirror to get a plane wavefront beam. The collimated wavefront is spatially divided in two parts: one directly impinges on the crystal sample; the other one impinges on the grating in a symmetric way, but after being reflected off the mirror M. As shown in the inset b of Fig. 1, the angle of incidence θ is chosen so that the two first-order diffracted wavefronts come out at an angle β with respect to the normal to the grating, with β depending on the period p of the

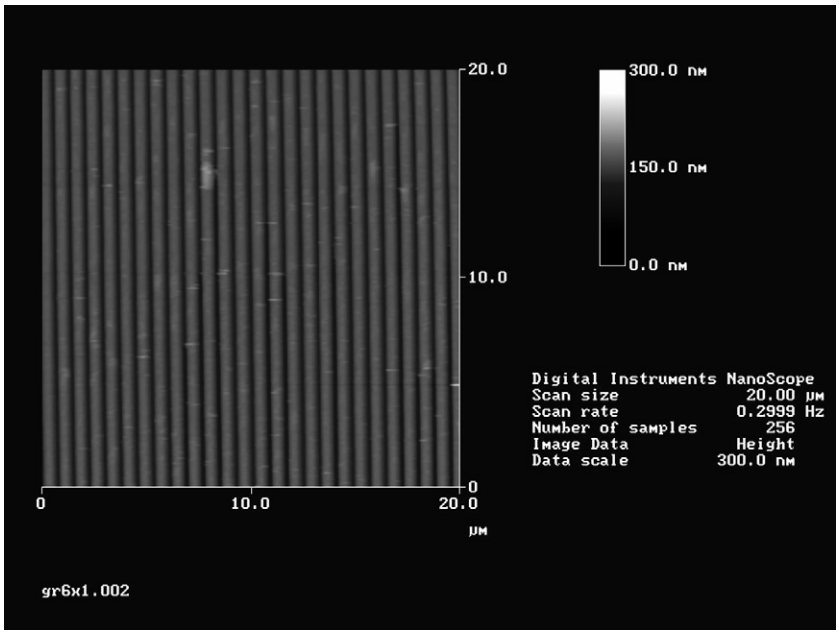

Fig. 2. Atomic force microscope image of a 20-μm-size square portion of the grating written on KTP sample. The grey scale goes from 0 to 300 nm.

grating and the wavelength λ of the light through the grating equation [19],

$$\sin\beta = \sin\theta - \lambda/p.$$

The two outcoming wavefronts give rise to a nonlocalized pattern of equally spaced moiré fringes [13], whose spatial frequency depends on the period of the grating through the angle β, as

$$\mathscr{F} = 2\sin\beta/\lambda.$$

The fringe pattern is recorded by a CCD camera, stored in a PC and successively analysed.

As the sample is heated, its length L along the monitored axis direction changes according to the thermal expansion law, which can be written as

$$L(T) = L_0[1 + \alpha(T)(T - T_0)], \tag{1}$$

where L_0 is the sample length at a reference temperature T_0 (hereafter assumed as 25 °C), and $\alpha(T)$ is the temperature-dependent mean thermal expansion coefficient [18]. If we assume that the grating follows the uniform expansion of the substrate, the spatial frequency $f = 1/p$ of the grating changes as

$$f(T) = \frac{f_0}{1 + \alpha(T)}(T - T_0),$$

where $f_0 = f(T_0)$ is the spatial frequency at temperature T_0. Assuming that the relative length variation due to thermal expansion is small, i.e., $\alpha(T)(T - T_0) \ll 1$, we get the fringe frequency as a function of the temperature

$$\begin{aligned}\mathscr{F}(T) &= \mathscr{F}_0 + 2f_0\alpha(T)(T - T_0) \\ &\simeq \mathscr{F}_0 + 2f_0[\alpha_0(T - T_0) + \alpha_1(T - T_0)^2],\end{aligned} \tag{2}$$

where $\mathscr{F}_0 = 2\sin\beta_0/\lambda$ is the fringe frequency at T_0, and a series-expansion is assumed in the last expression for the thermal expansion coefficient, $\alpha(T) = \alpha_0 + \alpha_1(T - T_0)$, limited to the first two terms.

3. Discussion of results

The optical setup is initially aligned in a symmetric configuration, such that both wavefronts are diffracted along the normal to the reflective grating, i.e., $\beta_0 = 0$. In this condition the interference pattern of the diffracted beams is null, i.e., $\mathscr{F}_0 = 0$. However, the symmetry of the incidence angles is not necessary and Eq. (2) holds in a more general case. Thus, we slightly tilt the mirror M so as to have an initial non-null moiré pattern, i.e., $\mathscr{F}_0 \neq 0$. We remark that $\mathscr{F}_0$ is just a free parameter to be determined by the fit procedure described below, and not necessarily corresponds to a particular experimental fringe pattern. Moreover, the effect of the thermal expansion on the fringe frequency does not depend on the initial moiré pattern neither on $\mathscr{F}_0$, as it is evident in Eq. (2). As a consequence, the initial pattern can be chosen simply by convenience, in such a way to have already a sufficient fringe frequency to start with, thus reducing the relative uncertainty and avoiding the influence of slowly varying modulation which could affect the recorded pattern. By comparison of Eqs. (1) and (2), we finally notice that a temperature change causes a relative variation of the sample length, as in Eq. (1), giving rise to an absolute fringe frequency change in Eq. (2). Thus, this is independent of the sample length, besides of the initial pattern, as mentioned above, and is scaled with respect to the relative displacement by the factor $2f_0$, depending only on the grating period. This feature allows investigation of very small samples, in principle as small as the

useful grating area, without reducing the sensitivity of the technique. However, the dimension of the grating cannot be reduced without affecting resolution, as this depends on the number of grating lines.

Once the crystal is placed on the holder and the interferometer is carefully aligned, the temperature of the holder is successively stabilized at different values between 25 and 200 °C, and for each temperature a fringe pattern (see Fig. 3a and b) is recorded by the CCD camera and stored in a PC. Each fringe pattern is analysed considering single rows in the expansion direction, i.e., perpendicular to the fringes. The intensity profile of each row is Fourier transformed and filtered. Then we recover the unwrapped phase [20] and, as a consequence, the number of fringe along the expansion direction can be plotted as in Fig. 3c. The slope of the plotted curve gives the spatial fringe frequency. The procedure is repeated for several rows, finally taking the average of the retrieved fringe frequencies.

The main source of uncertainty is given by the small imperfections of the grating which reflect in the recorded wavefront and can be estimated by the data dispersion of the fringe number as retrieved by different rows of the same interferogram. Possible sample tilt were checked during heating, giving a negligible contribution. We also estimated other sources of errors, due to beam collimation, local heating of the air, and aperture diffraction, however they give contributions which are negligible.

The data are then fitted by a parabolic curve, Eq. (2), determining the coefficient α_0 and α_1 along with the unused value for $\mathscr{F}_0$. The experimental error associated to each experimental data of the spatial fringe frequency is twice the standard deviation resulting from averaging over different rows of an interferogram. Fig. 4 shows measured fringe frequency versus the sample temperature, for two axis directions of the z-cut sample of KTP crystal. For a direct comparison we plotted each set of data and its best fit subtracted of the parameter $\mathscr{F}_0$, which is actually determined from the fitting procedure. In Table 1 we summarize the value obtained for different axes of our samples and the error reported for each coefficient is the error resulting from the fitting procedure by weighting the data with the experimental error as defined above.

For $LiNbO_3$ expansion coefficient several data were reported in the past years from measurements with different techniques [8]. Often the composition is not reported and discrepancies were found between different measurements. Also experimental point is often sparse over wide temperature intervals and errors on single data are omitted. One of the value currently reported by crystal producers

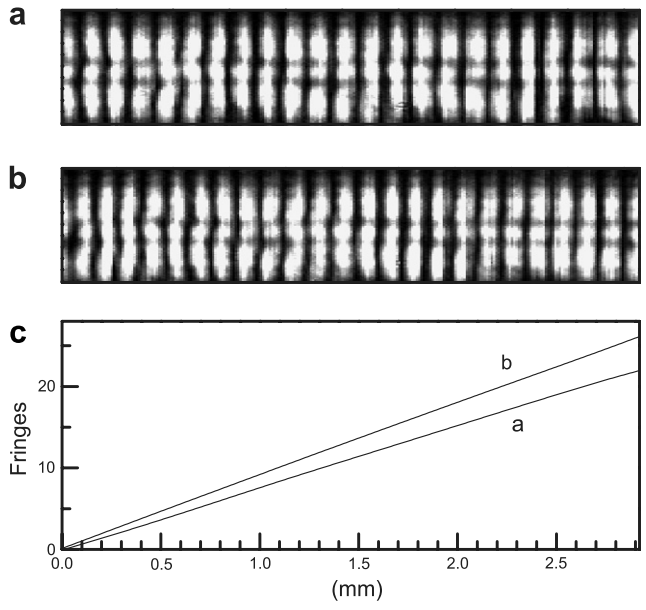

Fig. 3. Experimental patterns of moiré fringes along the x-axis of the KTP sample, recorded at 32.1 °C (a) and 99.0 °C (b) and (c) the corresponding number of fringes, as recovered from the analysis. The abscissas refer to the horizontal length of the fringe pattern and the spatial fringe frequency $\mathscr{F}$ is given by the slope of the lines.

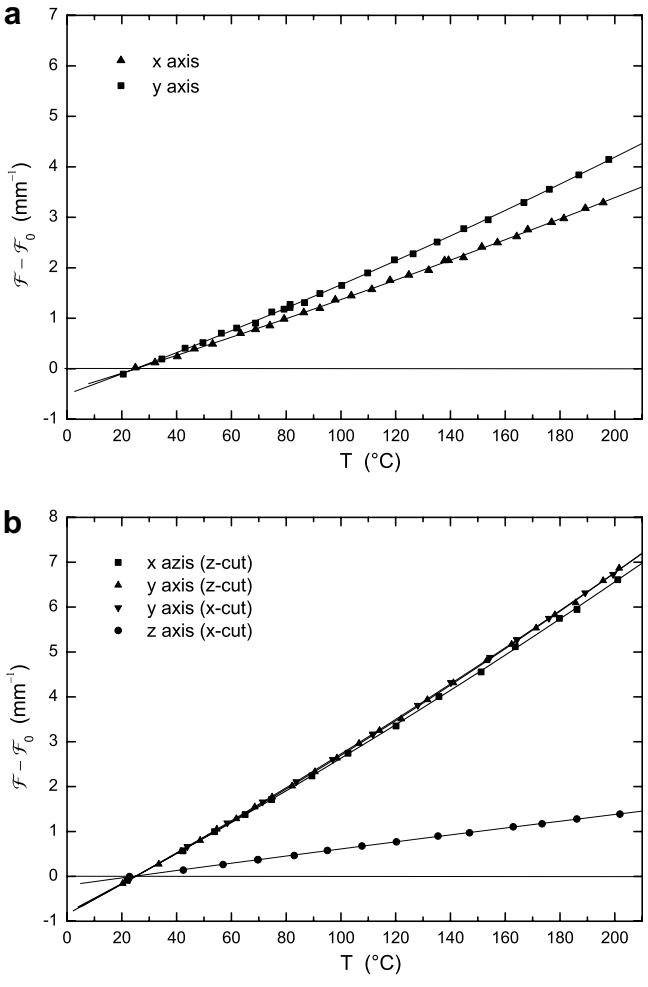

Fig. 4. Experimental values of the spatial fringe frequency of the moiré pattern as a function of the temperature for (a) z-cut KTP and (b) z-cut and x-cut $LiNbO_3$ samples. The experimental data are fitted by a parabolic curve (solid lines), according to Eq. (2). For comparison each set of data have been subtracted of the fringe frequency at 25 °C as given by the fitting procedure.

Table 1
Series-expansion coefficients of thermal expansion for different axes of KTP and $LiNbO_3$, between 20 and 200 °C

	α_0 (K^{-1})	α_1 (K^{-2})
KTP		
x-axis	$(7.0 \pm 0.2) \times 10^{-6}$	$(4.4 \pm 0.8) \times 10^{-9}$
y-axis	$(8.2 \pm 0.2) \times 10^{-6}$	$(7.1 \pm 0.8) \times 10^{-9}$
$LiNbO_3$		
x-axis	$(13.3 \pm 0.2) \times 10^{-6}$	$(9.7 \pm 1.0) \times 10^{-9}$
y-axis	$(13.6 \pm 0.2) \times 10^{-6}$	$(11.0 \pm 0.6) \times 10^{-9}$
y-axis	$(13.4 \pm 0.2) \times 10^{-6}$	$(9.2 \pm 0.6) \times 10^{-9}$
z-axis	$(3.4 \pm 0.2) \times 10^{-6}$	$(-1.0 \pm 0.6) \times 10^{-9}$

make reference to a measurement by X-ray diffraction [9] which found a different value for *x*- and *y*-axis. Ref. [8] combined different data from previous measurement, for different composition and fit them with a third order polynomial. For *x*- and *y*-axis, if we restrain to the 20–200 °C temperature interval and report their data to a second-order polynomial and to the same reference temperature $T_0 = 25$ °C, we get $14.5 \times 10^{-6}\,K^{-1}$ and $12.2 \times 10^{-9}\,K^{-2}$. Similarly for the *z*-axis, we get $4.5 \times 10^{-6}\,K^{-1}$ and $-1.5 \times 10^{-6}\,K^{-1}$. Our results are in good agreement with those values.

As far KTP is concerned, values previously reported, assuming constant thermal expansion coefficient, i.e. $\alpha(T) = \alpha_0$, were measured with different methods and in different temperature ranges: with a dilatometer between 20 and 100 °C [10], and with X-ray diffractometry from room temperature up to 700 °C [11]. There is a clear discrepancy between their results, which can be partially explained by the different temperature ranges. For a direct comparison with Ref. [10] we consider only the data between 20 and 100 °C and linearly fit them. We find $7.3(2) \times 10^{-6}\,K^{-1}$ and $8.7(2) \times 10^{-6}\,K^{-1}$ for the *x*- and *y*-axis respectively, in good agreement with the corresponding values reported in Ref. [10], as $6.8 \times 10^{-6}\,K^{-1}$ and $9.6 \times 10^{-6}\,K^{-1}$. A more recent and accurate measurement, giving also the second series-expansion coefficient α_2, was reported in Ref. [12], for the same temperature range of this paper, even though only for *x*-axis, giving $\alpha_0 = 6.7(7) \times 10^{-6}\,K^{-1}$ and $\alpha_1 = 11(2) \times 10^{-9}\,K^{-2}$. In this case the agreement is good for the first series coefficient, while a discrepancy occurs for the second series-expansion coefficient.

4. Conclusions

We have measured the thermal expansion coefficient of three samples of $LiNbO_3$ and KTP crystals by means of an interferometric setup which allows accurate estimate of the thermal expansion even for small-size sample (<10 mm). We determined the thermal expansion coefficients for the *x*, *y* and *z* crystal axes for $LiNbO_3$, while only *x*, *y* axes for KTP, as we had only a *z*-cut sample for it. The measurements were performed from room temperature up to 200 °C. The technique can be extended to other materials, provided that a grating can be written on the sample, following accurately the expansion of the sample itself. The setup can be easily upgraded in order to investigate also the thermal behaviour at different ranges of temperature, specially that below 0 °C.

Acknowledgements

The authors thank Alexander Tsukernik and Boris Kagan for their assistance. This research was partially funded by the Ministero dell'Istruzione dell'Universitáe della Ricerca (MIUR), Project MIUR No. 77 DD N.1105/2002, Israel Science Foundation, Grant No. 960/05, and by UE contract: RII3-CT-2003-506350.

References

[1] J.A. Armstrong, N. Bloembergen, J. Ducuing, P.S. Pershan, Phys. Rev. 127 (1962) 1918.
[2] P.A. Franken, J.F. Ward, Rev. Mod. Phys. 35 (1963) 23.
[3] J.D. Bierlein, H. Vanherzeele, J. Opt. Soc. Am. B 6 (1989) 622.
[4] K. Fradkin, A. Arie, A. Skliar, G. Rosenman, Appl. Phys. Lett. 74 (1999) 914.
[5] D.R. Wiese, U. Stroessner, A. Peters, J. Mlynek, R. Schiller, A. Arie, A. Skliar, G. Rosenman, Opt. Commun. 184 (2000) 329.
[6] C. Canalias, V. Pasiskevicius, M. Fokine, F. Laurell, Appl. Phys. Lett. 86 (2005) 181105.
[7] J. Mangin, P. Strimer, L. Lahlou-Kassi, Meas. Sci. Technol. 4 (1993) 826.
[8] D. Taylor, Thermal expansion coefficients of $LiNbO_3$, in: K.K. Wong (Ed.), Properties of Lithium Niobate, Inspec, London, 2002, and reference therein.
[9] Y.S. Kim, R.T. Smith, J. Appl. Phys. 40 (1969) 4637.
[10] D.K.T. Chu, J.D. Bierlein, R.G. Hunsperger, IEEE Trans. Ultrason. Ferroelectr. Freq. Control 39 (1992) 683.
[11] P. Delarue, C. Lecomte, M. Jannin, G. Marnier, B. Menaert, J. Phys.: Condens. Matter 11 (1999) 4123.
[12] S. Emanueli, A. Arie, Appl. Opt. 42 (2003) 6661.
[13] D. Post, Moiré interferometry, in: A.S. Kobayashi (Ed.), Handbook on Experimental Mechanics, John Wiley and Sons, New York, 1993.
[14] S. De Nicola, P. Ferraro, A. Finizio, G. Pierattini, Appl. Opt. 38 (1999) 4845.
[15] S. De Nicola, P. Ferraro, A. Finizio, G. Pesce, G. Pierattini, Opt. Commun. 118 (1995) 491.
[16] B. Han, Y. Guo, IEEE Trans. Comp. Pack. Manuf. Technol. 19 (1996) 240.
[17] B. Han, Z. Wu, S. Cho, Exp. Thechn. 25 (2001) 22.
[18] J.D. James, J.A. Spittle, S.G.R. Brown, R.W. Evans, Meas. Sci. Technol. 12 (2001) R1.
[19] M. Born, E. Wolf, Principles of Optics, Cambridge University Press, Cambridge, 2002.
[20] S. De Nicola, P. Ferraro, J. Opt. A 2 (2000) 228.